Adaptive anti-saturation fault-tolerant control for integrated missile guidance and control

*Peng Li[1], Qi Liu[1], Chen-Yu He and Xiao-qing Liu[2]**

1.The School of Information and Engineering at Xiangtan University，Hunan Changshan ,411100，China

2. Department of Precision Instruments, Tsinghua Universit javascript*, 100084, Beijing, China*

Abstract: This paper studies the integrated design problems of control and guidance with parameter uncertainties, target disturbances, input constraints and actuator faults. Firstly, based on the integrated design idea of the missile guidance and control, the auxiliary variable is used to establish and transform it into a cascade system with input constraints, actuator faults and disturbances of unknown upper bounds. Secondly, the adaptive anti-saturation dynamic surface fault-tolerant controller is designed by using the back-stepping method, adaptive control, auxiliary system and tracking differentiator. By introducing the tracking differentiator and tangent barrier Lyapunov function, the computational explosion problem in the traditional back-stepping method is avoided and the angle of attack can be guaranteed in prospective range, respectively. Finally, the theoretical proof of the designed control strategy is given to ensure that the states of the closed-loop system are bounded. At the same time, the digital simulation of the maneuvering target of different maneuvering forms is carried out, which further illustrate the effectiveness and robustness of the designed control schemes.

Keywords: Missile guidance and control; Dynamic surface control; state constraints; Input saturation; Actuator faults

1. Introduction

The design of the missile guidance and control system is the key factor for the missile flight success and accurate strike [1]. In the tradi[1]tional missile design method, the interaction between the guidance system and the control system is often neglected. When it is flying at big angles of attack and aimed at intercepting large maneuvering targets, the coupling relationship between the guidance and control systems may cause the degradation of the system performance, and even the failure of intercepting missions [2]. Therefore, the design method of integrated guidance and control has attracted the

Associate Professor Xiangtan University, email: pengli@xtu.edu.cn.
Ph.D. Student, Xiangtan University, email: 201821562120@smail.xtu.edu.cn.
Ph.D. Student, Xiangtan University, email: 201821562112@smail.xtu.edu.cn.
Ph.D. Student, Tsinghua Universit, email: lxq17@mails.tsinghua.edu.cn.

attention of many scholars.

In recent years, the nonlinear control theory has been widely used in the integrated guidance and control of flight control systems [3-6]. In [6], the adaptive dynamic surface sliding mode control law was designed based on the integrated guidance and control model of missile pitch channel to improve the missile guidance precision. In [7-8], the integrated guidance and control law was designed by using the sliding mode control and back-stepping control. In [9], the integrated model of guidance and control was transformed into the block diagonal model of attitude and velocity subsystem. Based on the sliding mode control theory and fuzzy control theory, the analytical solution of block diagonal combination was obtained. In [10-11], for the integrated model of missile guidance and system, the integrated controller of guidance and control was designed through the adaptive control technology and neural network theory. Integrated missile guidance and control with state constraints in practical systems[12]. In [13], in order to avoid the influence large angle of attack, flight strategy with angle-limited was designed. In [14-15], the back-stepping control with states constraints was designed for nonlinear systems constrained by using barrier Lyapunov function. In [16], the adaptive back-stepping controllers with state constraints was proposed for hypersonic vehicle. In [17], an adaptive dynamic surface controller was proposed for systems with state constraints by using the differentiator and barrier Lyapunov function.

In the actual design process of control system, the input saturation problem must be considered [18-20], If the input constraint is not considered in the controller design, the actuator may be saturated during the actual execution of the control law, which may lead to the degradation of the guidance performance or even the instability of the guidance system. In [21-22], an anti-saturation adaptive back-stepping controller was designed by introducing an instruction constraint system. In [23-24], the guidance law was designed through the adaptive technology and auxiliary systems, which can solve the input saturation problem. In addition, due to the external disturbances, model parameter uncertainties and input saturation of the missile guidance and control system, which can more likely to lead to actuator fault. In [25], the dynamic surface fault-tolerant controller was proposed by using the extended state observer and dynamic surface control method. In [26]， an adaptive back-stepping sliding mod fault-tolerant controller was proposed for integrated guidance and control system. In [27], an adaptive fault-tolerant controller was provided for the integrated guidance and control system with state constraints and actuator faults, however the input saturation is not considered. In order to further solve

the problem of integrated missile guidance and control, this paper aims at the integrated control model of the missile pitch plane and maneuver target with unknown upper bound. Based on the dynamic surface control, adaptive control technology, auxiliary system and tangent barrier Lyapunov function, the adaptive anti-saturation fault-tolerant controller is designed, which can make the angle of attack satisfying in prospective ranges. Compared with the existing works, the main contributions of the thesis are shown as follows:

(1) A novel tracking differentiator filter is developed in conjunction with the back-stepping control that eliminates the complexity problem.

(2) The tangent barrier Lyapunov function is introduced in the adaptive fault-tolerant control strategy to guarantee the angle of attack keep within the certain ranges.

(3) Input saturation, actuator faults and state constraints are taken into account to design controller, which makes the designed controllers have practical significance.

The structure of the rest of the thesis is organized in following manner. Section 2 presents an integrated guidance and control system model. Section 3, an adaptive anti-saturation dynamic surface fault-tolerant controller is proposed. Section 4 gives numerical simulations of the proposed controllers. In Section 5, the conclusion of the thesis is presented.

2. Problem statements

The two-dimensional plane intercept geometry of the missile-target is shown in Fig.1, The M and T represent the missile and target respectively. The dynamic equation of the relative motion of the missile-target can be obtained [6].

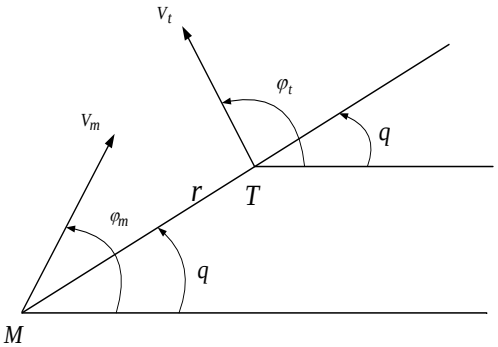

Fig.1. Two-dimensional engagement geometry

$$\dot{r} = V_t \cos(q - \varphi_t) - V_m \cos(q - \varphi_m) \tag{1}$$

$$r\dot{q} = -V_t \sin(q - \varphi_t) + V_m \sin(q - \varphi_m) \tag{2}$$

$$\dot{\varphi}_t = a_t / V_t \tag{3}$$

$$\dot{\varphi}_m = a_m / V_m \tag{4}$$

where r and q represent relative distance and line-of-sight angle, respectively. $\dot{r}$ and $\dot{q}$ denote relative

velocity and line-of-sight angular rate. V_M, φ_m and a_m represent velocity, flight path angle and lateral accelerations of the missile, respectively. V_t, φ_t and a_t denote velocity, flight path angle and lateral accelerations of the target respectively.

Computing the first order derivative of (2), yields

$$\begin{aligned} \dot{r}\dot{q}+r\ddot{q}=-\dot{q}[V_t\cos(q-\varphi_t)-V_m\cos(q-\varphi_m)]+ \\ V_t\dot{\varphi}_t\cos(q-\varphi_t)-V_m\dot{\varphi}_m\cos(q-\varphi_m) \end{aligned} \tag{5}$$

Let $V_q=r\dot{q}$, $a_t=V_t\dot{\varphi}_t$, $a_m=V_M\dot{\varphi}_m$, using (1)-(4) can be derived

$$\dot{V}_q=-\frac{\dot{r}}{r}V_q+a_t\cos(q-\varphi_t)-a_m\cos(q-\varphi_m) \tag{6}$$

Refer to [11], the differential equations of pitch motion can be described as

$$mV_M\frac{d\varphi_M}{dt}=Y-mg\cos\varphi_M \tag{7}$$

$$J_z\frac{dw_z}{dt}=M_z \tag{8}$$

$$\frac{dx}{dt}=V_M\cos\varphi_M \tag{9}$$

$$\frac{dv}{dt}=w_z \tag{10}$$

$$\alpha=v-\theta_M \tag{11}$$

From (7), we can have

$$a_M=V_M\dot{\varphi}_M=\frac{1}{m}\left(Y-mg\cos\varphi_M\right) \tag{12}$$

Substituting (12) into (6) yields:

$$\dot{V}_q=-\frac{\dot{r}}{r}V_q+a_T\cos\left(q-\varphi_T\right)-\frac{1}{m}\left(Y-mg\cos\varphi_M\right)\cos\left(q-\varphi_M\right) \tag{13}$$

Based on (10) and (11) can be rearranged as

$$\dot{\alpha}=w_z-\frac{1}{mV_M}\left(Y-mg\cos\varphi_M\right) \tag{14}$$

According to (8), we get

$$\frac{dw_z}{dt}=\frac{M_z}{J_z} \tag{15}$$

The lift force and pitching moment of the missile are defined as

$$Y=57.3qs\left(c_y^{\alpha}\alpha+c_y^{\delta_z}\delta_z\right) \tag{16}$$

$$M_z=\frac{qsl^2m_z^{\bar{w}_z}}{V_M}w_z+57.3qslm_z^{\alpha}\alpha+57.3qslm_z^{\delta_z}\delta_z \tag{17}$$

Substituting (16)-(17) into (13)-(15) and applying $\cos\left(q-\varphi_M\right)\approx 1$, The following integrated guidance and control model can be derived

$$\dot{V}_q=-\frac{\dot{r}}{r}V_q-\frac{57.3qsc_y^a}{m}\alpha+g\cos\varphi_m\cos\left(q-\varphi_m\right)+d_{Vq} \tag{18}$$

$$\dot{\alpha} = -\frac{57.3qsc_y^a}{mV_M}\alpha + w_z + \frac{g\cos\varphi_m}{V_M} + d_\alpha \tag{19}$$

$$\dot{w}_z = -\frac{57.3qslm_z^a}{J_z}\alpha + \frac{qsl^2m_z^{\bar{w}_z}}{J_zV_M}w_z + \frac{57.3qslm_z^{\delta_z}}{J_z}\delta_z + d_{wz} \tag{20}$$

where d_{Vq}, d_α and d_{wz} are the bounded terms produced by parameter uncertainties, aerodynamic uncertainties and external disturbances.

Let

$$\begin{aligned} &\alpha_{11} = -\frac{\dot{r}}{r}, \alpha_{12} = -\frac{57.3qsc_y^\alpha}{m}, \alpha_{22} = -\frac{57.3qsc_y^\alpha}{mV_M} \\ &\alpha_{32} = \frac{57.3qsm_z^\alpha}{J_z}, \alpha_{33} = \frac{qsl^2m_z^{\bar{w}_z}}{J_zm}, b = \frac{57.3qsl^2m_z^{\delta_z}}{J_z} \end{aligned} \tag{21}$$

According to (21), then (18)-(20)can be rewritten as:

$$\dot{V}_q = \alpha_{11}V_q + \alpha_{12}\alpha + g\cos\varphi_m\cos(q-\varphi_m) + d_{Vq} \tag{22}$$

$$\dot{\alpha} = \alpha_{22}\alpha + w_z + \frac{g\cos\varphi_m}{V_M} + d_\alpha \tag{23}$$

$$\dot{w}_z = \alpha_{32}\alpha + \alpha_{33}w_z + b\delta_z + d_{wz} \tag{24}$$

Further, then(22)-(24) can be derived as

$$\dot{x}_1 = f_1(x_1) + x_2 + \Delta_1(x_2) \tag{25}$$

$$x_2 = f_2(x_2) + x_3 + \Delta_2(x_2) \tag{26}$$

$$\dot{x}_3 = f_3(x_3) + bu + \Delta_3(x_2, x_3, u) \tag{27}$$

where $x_1 = V_q/\alpha_{12}$, $x_2 = \alpha$, $x_3 = w_z$, $u = \delta_z$, $\Delta_1(x_2) = d_{Vq}/\alpha_{12}$, $\Delta_2 = d_\alpha$, $\Delta_3 = d_{wz}$, $f_1(x_1) = \alpha_{11}x_1 + g\cos\varphi_m\cos(q-\varphi_m)$, $f_2(x_2) = \alpha_{22}x_2 + \frac{g\cos\varphi_m}{V_M}$, $f_3(x_3) = \alpha_{32}x_2 + \alpha_{33}x_3$.

In this paper, the following actuator-fault model and input saturation of missile are considered

$$u = \rho\,\mathrm{sat}(v) + \bar{u} \tag{28}$$

where v is the fin deflection command to be determined, $0 < \rho < 1$ denotes the actuation effectiveness, $\bar{u}$ is the additive fault.

Considering (28) the integrated guidance and control model can be rewritten as

$$\dot{x}_1 = f_1(x_1) + x_2 + \Delta_1(x_1) \tag{29}$$

$$x_2 = f_2(x_2) + x_3 + \Delta_2(x_1, x_2) \tag{30}$$

$$\dot{x}_3 = f_3(x_3) + b(\rho\,\mathrm{sat}(v) + \bar{u}) + \Delta_3(x_1, x_2, x_3, u) \tag{31}$$

Assumption 1: The external disturbances $\Delta_1(x_1)$, $\Delta_2(x_1, x_2)$ and $\Delta_3(x_2, x_3, u)$ in(29)-(31) are assumed to be bounded, and satisfy the following condition

$$\left|\Delta_1(x_1)\right| \le M_1, \left|\Delta_2(x_1,x_2)\right| \le M_2, \left|\Delta_3(x_1,x_2,x_3,u)\right| \le M_3 \tag{32}$$

where M_1, M_2 and M_3 are unknown positive constants.

Lemma 1: For $n+1$ order tracking differentiator(33), if the input signal α_r contains a bounded noise $|\chi_1-\alpha_r| \le \kappa$, there exist positive constant v_i, $\bar{r}_i$ that make inequality (34) hold:

$$\begin{cases} \dot{\chi}_1 = -r_1 \left|\chi_1-\alpha_r\right|^{\frac{n}{n+1}} \operatorname{sign}(\chi_1-\alpha_r)+\chi_2 \\ \cdots \\ \dot{\chi}_i = -r_i \left|\chi_i-\dot{\chi}_{i-1}\right|^{\frac{n+1-i}{n+2-i}} \operatorname{sign}(\chi_i-\dot{\chi}_{i-1})+\chi_{i+1} \\ \cdots \\ \dot{\chi}_n = -r_n \left|\chi_n-\dot{\chi}_{n-1}\right|^{\frac{1}{2}} \operatorname{sign}(\chi_n-\dot{\chi}_{n-1})+\chi_{n+1} \\ \dot{\chi}_{n+1} = -r_n \operatorname{sign}(\chi_{n+1}-\dot{\chi}_n) \end{cases} \tag{33}$$

$$\begin{aligned} \left|\chi_i-\alpha_{ri}\right| &\le v_i \kappa^{\frac{n+2-i}{n+1}}, i=1,2,\ldots,n \\ \left|\upsilon_j-\alpha_{r(j+1)}\right| &\le \bar{r}_j \kappa^{\frac{n+1-j}{n+1}}, j=1,2,\ldots,n-1 \end{aligned} \tag{34}$$

where r_i ($i=1,2,\ldots,n+1$) is positive constant, $\alpha_{r(j+1)}$ represents j order differential of α_r.

3. Controller Design

The adaptive anti-saturation dynamic surface fault-tolerant controller is design for the integrated guidance model based on the back-stepping method, tracking differentiators, adaptive control, auxiliary system and tangent barrier Lyapunov function, which can guarantee the angle of attack meets the actual constraint requirements.

Step1: Define the error variable z_1 as follows:

$$z_1 = x_1 - x_{1c} \tag{35}$$

where x_{1c} is reference signal.

Computing the derivative of (35), it can be obtained that

$$\dot{z}_1 = \dot{x}_1 - \dot{x}_{1c} = f_1(x_1) + x_2 + \Delta_1(x_2) - \dot{x}_{1c} \tag{36}$$

According to (36), the virtual control $\bar{x}_2$ is designed as follows

$$\bar{x}_2 = -f_1(x_1) - k_1 z_1 - k_2 \operatorname{sig}^{\gamma_1}(z_1) + \hat{M}_1 \operatorname{sign}(z_1) + \dot{x}_{1c} \tag{37}$$

$$\dot{\hat{M}}_1 = p_1\left(|z_1| - l_1 \hat{M}_1\right) \tag{38}$$

where k_1, k_2, p_1 and l_1 are positive constants, $0<\gamma_1<1$.

Choose the Lyapunov function as

$$V_1 = \frac{1}{2} z_1^2 + \frac{1}{2p_1} \tilde{M}_1^{\,2} \tag{39}$$

where $\tilde{M}_1 = M_1 - \hat{M}_1$ is the estimation error of adaptive parameter

Applying (37) and(38), the time derivative of the (39) can be written as

$$\begin{aligned}\dot{V}_1 &= z_1\left(f_1(x_1)+z_2+\bar{x}_2+\Delta_1(x_2)-\dot{x}_{1c}\right)-\frac{1}{p_1}\tilde{M}_1\dot{\hat{M}}_1\\ &= -k_1z_1^2-k_2z_1\,\mathrm{sig}^{\gamma_1}(z_1)+z_1z_2+z_1\left(\Delta_1(x_2)-\hat{M}_1\,\mathrm{sign}(z_1)\right)-\frac{1}{p_1}\tilde{M}_1\dot{\hat{M}}_1\\ &\le -k_1z_1^2-k_2z_1\,\mathrm{sig}^{\gamma_1}(z_1)+z_1z_2+z_1\left(M_1-\hat{M}_1\,\mathrm{sign}(z_1)\right)-\frac{1}{p_1}\tilde{M}_1\dot{\hat{M}}_1\\ &\le -k_1z_1^2-k_2z_1\,\mathrm{sig}^{\gamma_1}(z_1)+z_1z_2+|z_1|\tilde{M}_1-\tilde{M}_1\left(|z_1|-l_1\hat{M}_1\right)\\ &\le -k_1z_1^2-k_2z_1\,\mathrm{sig}^{\gamma_1}(z_1)+z_1z_2+l_1\hat{M}_1\tilde{M}_1\\ &\le -k_1z_1^2-k_2z_1\,\mathrm{sig}^{\gamma_1}(z_1)-\frac{1}{2}l_1\tilde{M}_1^2+z_1z_2+\frac{1}{2}l_1M_1^2\end{aligned} \tag{40}$$

To avoid the derivative of virtual controller $\bar{x}_2$, the tracking differentiator (41) is introduced as

$$\begin{cases}\dot{\chi}_{2,1}=-r_1\left|\chi_{2,1}-\bar{x}_2\right|^{\frac{1}{2}}\mathrm{sign}\left(\chi_{2,1}-\bar{x}_2\right)+\chi_{2,2}\\ \dot{\chi}_{2,2}=-r_2\,\mathrm{sign}(\chi_{2,2}-\dot{\chi}_{2,1})\end{cases} \tag{41}$$

where r_1 and r_2 are positive constants.

Apply Lemma1, inequality (42) can be obtained:

$$\left|\chi_{2,1}-\bar{x}_2\right|\le= l_{2,1}\,,\left|\dot{\chi}_{2,1}-\dot{\bar{x}}_2\right|\le= l_{2,2} \tag{42}$$

where $l_{2,1}$ and $l_{2,2}$ are positive constants.

Step2: Define the error variable z_2 as follows:

$$z_2 = x_2-\bar{x}_2 \tag{43}$$

The derivative of (43) can be written as

$$\dot{z}_2=\dot{x}_2-\dot{\bar{x}}_2=f_2(x_2)+x_3+\Delta_2(x_2)-\dot{\bar{x}}_2 \tag{44}$$

To guarantee the angle of attack satisfying $|z_2|\le A$ with $A>0$ being positive constants, respect to (44), the virtual control $\bar{x}_3$ is designed as follows

$$\begin{aligned}\bar{x}_3 &= -k_3\frac{A^2}{z_2\pi}\sin\left(\frac{\pi z_2^2}{2A^2}\right)\cos\left(\frac{\pi z_2^2}{2A^2}\right)-f_2(x_2)\\ &\quad-\frac{1}{\tau}\left(k_{30}z_2-z_2z_1+\hat{M}_2\,\mathrm{sign}(\tau)+\dot{\chi}_{2,1}-\hat{l}_{2,2}\,\mathrm{sign}(\tau)\right)\end{aligned} \tag{45}$$

$$\begin{aligned}\dot{\hat{M}}_2 &= p_2\left(|z_2|-l_2\hat{M}_2\right)\\ \dot{\hat{l}}_{2,2} &= p_3\left(|z_2|-l_3\hat{l}_{2,2}\right)\end{aligned} \tag{46}$$

where k_3, k_{30} k_4 p_2, p_3, l_2 and l_3 are positive constants, $k_3>k_{30}$, $k_{30}=\sqrt{\left(\frac{\dot{A}}{A}\right)^2+o}$, o is positive constant, $0<\gamma_2<1$

The tangent barrier Lyapunov function is designed as

$$V_2 = \frac{A^2}{\pi}\tan\left(\frac{\pi z_2^2}{2A^2}\right) + \frac{1}{2p_2}\tilde{M}_2^{\,2} + \frac{1}{2p_3}\tilde{l}_{2,2}^{\,2} \tag{47}$$

where $\tau = z/\cos^2\left(\frac{\pi z_2^3}{2A^2}\right)$, $\tilde{M}_2 = M_2 - \hat{M}_2$ and $\tilde{l}_{2,2} = l_{2,2} - \hat{l}_{2,2}$.

The derivative of V_2 can be written as

$$\begin{aligned}\dot{V}_2 = {} & \frac{2A\dot{A}}{\pi}\tan\left(\frac{\pi z_2^2}{2A^2}\right) - \left(\frac{\dot{A}}{A}\right)\tau z_2 + \tau\left(f_2(x_2) + z_3 + \bar{x}_3 + \Delta_2(x_2) - \dot{\bar{x}}_2\right) \\ & - \frac{1}{p_2}\tilde{M}_2\dot{\hat{M}}_2 - \frac{1}{p_3}\tilde{l}_{2,2}\dot{\hat{l}}_{2,2}\end{aligned} \tag{48}$$

Substituting (45)-(46) into (48) yields:

$$\begin{aligned}\dot{V}_2 &= \frac{2A\dot{A}}{\pi}\tan\left(\frac{\pi z_2^2}{2A^2}\right) - \left(\frac{\dot{A}}{A}\right)\tau z_2 + \tau\left(f_2(x_2) + z_3 + \bar{x}_3 + \Delta_2(x_2) - \dot{\bar{x}}_2\right) - \frac{1}{p_2}\tilde{M}_2\dot{\hat{M}}_2 - \frac{1}{p_3}\tilde{l}_{2,2}\dot{\hat{l}}_{2,2} \\ &= \frac{2A\dot{A}}{\pi}\tan\left(\frac{\pi z_2^2}{2A^2}\right) - \left(\frac{\dot{A}}{A}\right)\tau z_2 - k_{30}z_2 + z_3\tau - z_1 z_2 + \tau\left(\Delta_2(x_2) - \hat{M}_2\,\mathrm{sign}(\tau)\right) \\ &\quad + \tau\left(\dot{\chi}_{2,1} - \dot{\bar{x}}_2 - \hat{l}_{2,2}\,\mathrm{sign}(\tau)\right) - \tau\left(k_3\frac{A^2}{z_2\pi}\sin\left(\frac{\pi z_2^2}{2A^2}\right)\cos\left(\frac{\pi z_2^2}{2A^2}\right)\right) - \frac{1}{p_2}\tilde{M}_2\dot{\hat{M}}_2 - \frac{1}{p_3}\tilde{l}_{2,2}\dot{\hat{l}}_{2,2}\end{aligned} \tag{49}$$

The following inequality can be derived

$$-k_3\tau\frac{1}{z_2}\frac{A^2}{\pi}\sin\left(\frac{\pi z_2^2}{2A^2}\right)\cos\left(\frac{\pi z_2^2}{2A^2}\right) = -k_3\frac{A^2}{\pi}\tan\left(\frac{\pi z_2^2}{2A^2}\right) \tag{50}$$

$$\frac{2A\dot{A}}{\pi}\tan\left(\frac{\pi z_2^2}{2A^2}\right) = \frac{2\dot{A}}{A}\frac{A^2}{\pi}\tan\left(\frac{\pi z_2^2}{2A^2}\right) \le \frac{2k_{30}A^2}{\pi}\tan\left(\frac{\pi z_2^2}{2A^2}\right) \tag{51}$$

Substituting (50)-(51) into (49) yields:

$$\begin{aligned}\dot{V}_2 \le {} & -k_3^*\frac{A^2}{\pi}\tan\left(\frac{\pi z_2^2}{2A^2}\right) + z_3\tau - z_1 z_2 + \tau\left(\Delta_2(x_2) - \hat{M}_2\,\mathrm{sign}(\tau)\right) \\ & + \tau\left(\dot{\chi}_{2,1} - \dot{\bar{x}}_2 - \hat{l}_{2,2}\,\mathrm{sign}(\tau)\right) - \frac{1}{p_2}\tilde{M}_2\dot{\hat{M}}_2 - \frac{1}{p_3}\tilde{l}_{2,2}\dot{\hat{l}}_{2,2}\end{aligned} \tag{52}$$

where $k_3^* = k_3 - 2k_{30}$.

According to (50)-(51), then (52) can be further simplified as

$$\begin{aligned}\dot{V}_2 &\le -k_3^*\frac{A^2}{\pi}\tan\left(\frac{\pi z_2^2}{2A^2}\right) + z_3\tau - z_1 z_2 + \tilde{M}_2|\tau| + \tilde{l}_{2,2}|\tau| - \tilde{M}_2\left(|\tau| - l_2\hat{M}_2\right) - \tilde{l}_{2,2}\left(|\tau| - l_3\hat{l}_{2,2}\right) \\ &\le -k_3^*\frac{A^2}{\pi}\tan\left(\frac{\pi z_2^2}{2A^2}\right) + z_3\tau - z_1 z_2 + l_2\hat{M}_2\tilde{M}_2 + l_3\tilde{l}_{2,2}\hat{l}_{2,2} \\ &\le -k_3^*\frac{A^2}{\pi}\tan\left(\frac{\pi z_2^2}{2A^2}\right) + z_3\tau - z_1 z_2 - \frac{1}{2}l_2\tilde{M}_2^2 - \frac{1}{2}l_3\tilde{l}_{2,2}^2 + \frac{1}{2}l_2 M_2^2 + \frac{1}{2}l_3 l_{2,2}^2\end{aligned} \tag{53}$$

To avoid the derivative of virtual controller $\bar{x}_3$, the tracking differentiator (54) is introduced as

$$\begin{cases}\dot{\chi}_{3,1} = -r_3\left|\chi_{3,1} - \bar{x}_3\right|^{\frac{1}{2}}\mathrm{sign}\left(\chi_{3,1} - \bar{x}_3\right) + \chi_{3,2} \\ \dot{\chi}_{3,2} = -r_4\,\mathrm{sign}(\chi_{3,2} - \dot{\chi}_{3,1})\end{cases} \tag{54}$$

where r_3 and r_4 are positive constants.

Apply Lemma1, as the following inequality holds:

$$\left|\chi_{3,1}-\bar{x}_3\right|\leq= l_{3,1},\ \ \left|\dot{\chi}_{3,1}-\dot{\bar{x}}_3\right|\leq= l_{3,2} \tag{55}$$

where $l_{3,1}$ and $l_{3,2}$ are positive constants.

Step3: Define the error variable z_3 as follows:

$$z_3=x_3-\bar{x}_3 \tag{56}$$

The derivative of (56) is given by

$$\dot{z}_3=\dot{x}_3-\dot{\bar{x}}_3=f_3\left(x_3\right)+b\left(\rho\,\mathrm{sat}\left(v\right)+\bar{u}\right)+\Delta_3\left(x_2,x_3,u\right)-\dot{\bar{x}}_3 \tag{57}$$

In order to solve the input constraint, the auxiliary system is designed as follows

$$\dot{\xi}=\begin{cases}-k_8\xi-\dfrac{\left|z_3b\rho\Delta v\right|+0.5b\Delta v^2}{\left|\xi\right|^2}\xi-b\Delta v-k_9\,\mathrm{sig}^{\gamma_3}(\xi), & \left|\xi\right|\geq\eta\\ 0, & \left|\xi\right|<\eta\end{cases} \tag{58}$$

where ξ is the state variable of the auxiliary system, k_8, k_9 and η are positive constants, $0<\gamma_3<1$, $\Delta v=\mathrm{sat}\left(v\right)-v_c$.

The adaptive anti-saturation dynamic surface fault-tolerant controller v_c is proposed as

$$v_c=-f_3\left(x_2\right)-k_5z_3-\tau z_2-k_6\,\mathrm{sig}^{\gamma_4}\left(z_3\right)-\hat{M}_3\,\mathrm{sign}\left(z_3\right)+\dot{\chi}_{3,1}-\hat{l}_{3,2}\,\mathrm{sign}\left(z_3\right)+k_7\xi \tag{59}$$

$$\begin{aligned}\dot{\hat{M}}_3&=p_4\left(\left|z_3\right|-l_4\hat{M}_3\right)\\ \dot{\hat{l}}_{3,2}&=p_5\left(\left|z_3\right|-l_5\hat{l}_{3,2}\right)\end{aligned} \tag{60}$$

$$\dot{\hat{\ell}}_V=p_6v_c-l_6\hat{\ell}_V \tag{61}$$

$$\dot{\hat{\chi}}=p_7z_3\tan\left(\frac{z_3}{\varepsilon}\right)-l_7\hat{\chi} \tag{62}$$

where k_5, k_6, k_7, p_5, p_4, p_6, p_7, l_4, l_5, l_6, l_7 and ε are positive constants, $0<\gamma_4<1$.

Theorem 1: Considering the system model (29)-(31)with Assumption1, then applying the guidance law (59), the line-of-sight angle rate $\dot{q}$ will converge to the region in finite time.

$$\boldsymbol{z}_{vi}\leq\sqrt{V\left(0\right)+\Gamma}=\Delta_i(i=1,2,3) \tag{63}$$

Poof：The Lyapunov function is chosen as follows

$$V=V_1+V_2+\frac{1}{2}z_3^2+\frac{1}{2p_4}\tilde{M}_3^{\ 2}+\frac{1}{2p_5}\tilde{l}_{3,2}^2+\frac{\lambda}{2p_6}\tilde{\ell}^2+\frac{1}{2p_7}\tilde{\chi}^2+\frac{1}{2}\xi^2 \tag{64}$$

where $\tilde{M}_3=M_3-\hat{M}_3$ $\tilde{l}_{3,2}=l_{3,2}-\hat{l}_{3,2}$, $\tilde{\ell}=\ell-\hat{\ell}$ and $\tilde{\chi}=\chi-\hat{\chi}$.

Let

$$V_3=\frac{1}{2}z_3^2+\frac{1}{2p_4}\tilde{M}_3^{\ 2}+\frac{1}{2p_5}\tilde{l}_{3,2}^2+\frac{1}{2}\xi^2 \tag{65}$$

Appling(59) the derivative of (65) can be obtained

$$
\begin{aligned}
\dot{V}_3 &= z_3\dot{z}_3 - \frac{1}{p_4}\tilde{M}_3\dot{\hat{M}}_3 - \frac{1}{p_5}\tilde{l}_{3,2}\dot{\hat{l}}_{3,2} - \frac{\lambda}{p_6}\tilde{\ell}\dot{\tilde{\ell}} - \frac{1}{p_7}\tilde{\chi}\dot{\tilde{\chi}} + \xi\dot{\xi} \\
&= z_3\left(f_3(x_3) + b\left(\rho\,\mathrm{sat}(v) + \bar{u}\right) + \Delta_3(x_2,x_3,u) - \dot{\bar{x}}_3\right) - \frac{1}{p_4}\tilde{M}_3\dot{\hat{M}}_3 - \frac{1}{p_5}\tilde{l}_{3,2}\dot{\hat{l}}_{3,2} - \frac{\lambda}{p_6}\tilde{\ell}\dot{\tilde{\ell}} - \frac{1}{p_7}\tilde{\chi}\dot{\tilde{\chi}} + \xi\dot{\xi} \\
&= z_3\left(f_3(x_3) + b\rho v_c + b\rho\Delta v + b\bar{u} + \Delta_3(x_2,x_3,u) - \dot{\bar{x}}_3\right) - \frac{1}{p_4}\tilde{M}_3\dot{\hat{M}}_3 - \frac{1}{p_5}\tilde{l}_{3,2}\dot{\hat{l}}_{3,2} - \frac{\lambda}{p_6}\tilde{\ell}\dot{\tilde{\ell}} - \frac{1}{p_7}\tilde{\chi}\dot{\tilde{\chi}} + \xi\dot{\xi} \\
&= z_3\left(f_3(x_3) + v_1 - v_1 + b\rho v_c + b\bar{u} + b\rho\Delta v + \Delta_3(x_2,x_3,u) - \dot{\bar{x}}_3\right) - \frac{1}{p_4}\tilde{M}_3\dot{\hat{M}}_3 - \frac{1}{p_5}\tilde{l}_{3,2}\dot{\hat{l}}_{3,2} - \frac{\lambda}{p_6}\tilde{\ell}\dot{\tilde{\ell}} - \frac{1}{p_7}\tilde{\chi}\dot{\tilde{\chi}} + \xi\dot{\xi} \\
&= -k_5 z_3^2 - k_6 z_3\,\mathrm{sig}^{\gamma_4}(z_3) - \tau z_3 z_2 + z_3 v_1 + z_3 b\rho v_c + z_3 b\bar{u} + z_3 b\rho\Delta v + z_3\left(\Delta_3(x_2,x_3,u) - \hat{M}_3\,\mathrm{sign}(z_3)\right) \\
&\quad + z_3\left(\dot{\chi}_{3,1} - \dot{\bar{x}}_3 - \hat{l}_{3,2}\,\mathrm{sign}(z_3)\right) + z_3 k_7\xi - \frac{1}{p_4}\tilde{M}_3\dot{\hat{M}}_3 - \frac{1}{p_5}\tilde{l}_{3,2}\dot{\hat{l}}_{3,2} - \frac{\lambda}{p_6}\tilde{\ell}\dot{\tilde{\ell}} - \frac{1}{p_7}\tilde{\chi}\dot{\tilde{\chi}} + \xi\dot{\xi} \\
&\le -k_5 z_3^2 - k_6 z_3\,\mathrm{sig}^{\gamma_4}(z_3) - \tau z_3 z_2 + z_3 v_1 + z_3 b\rho v_c + k_7\xi + z_3\left(\chi - \hat{\chi}\tan\left(\frac{z_3}{\varepsilon}\right)\right) + z_3 b\rho\Delta v \\
&\quad + z_3 k_7\xi + z_3\left(\Delta_3(x_2,x_3,u) - \hat{M}_3\,\mathrm{sign}(z_3)\right) + z_3\left(\dot{\chi}_{3,1} - \dot{\bar{x}}_3 - \hat{l}_{3,2}\,\mathrm{sign}(z_3)\right) \\
&\quad - \frac{\lambda}{p_6}\tilde{\ell}\dot{\tilde{\ell}} + \frac{1}{p_7}\tilde{\chi}\left(-\dot{\hat{\chi}} + p_7 z_3\tan\left(\frac{z_3}{\varepsilon}\right)\right) - \frac{1}{p_4}\tilde{M}_3\dot{\hat{M}}_3 - \frac{1}{p_5}\tilde{l}_{3,2}\dot{\hat{l}}_{3,2} + \xi\dot{\xi}
\end{aligned}
\tag{66}
$$

As

$$
z_3 b\rho v_c \le -\frac{\lambda\hat{\ell}v_{vc}^2}{\sqrt{\hat{\ell}v_c^2 + \delta_1}} \le \lambda\delta_1 - \lambda\hat{\ell}v_c \tag{67}
$$

$$
\chi\left(|z_3| - z_3\tan\left(\frac{z_3}{\varepsilon}\right)\right) \le \kappa\chi\varepsilon \tag{68}
$$

Substituting (67)-(68) into (66) yields

$$
\begin{aligned}
\dot{V}_3 &\le -k_5 z_3^2 - k_6 z_3\,\mathrm{sig}^{\gamma_4}(z_3) - \tau z_3 z_2 + z_3 v_1 + \lambda\delta_1 - \lambda\hat{\ell}v_c + k_7\xi + \kappa\chi\varepsilon + z_3 b\rho\Delta v \\
&\quad + z_3 k_7\xi + z_3\left(\Delta_3(x_2,x_3,u) - \hat{M}_3\,\mathrm{sign}(z_3)\right) + z_3\left(\dot{\chi}_{3,1} - \dot{\bar{x}}_3 - \hat{l}_{3,2}\,\mathrm{sign}(z_3)\right) \\
&\quad - \frac{\lambda}{p_6}\tilde{\ell}\dot{\tilde{\ell}} + \frac{1}{p_7}\tilde{\chi}\left(-\dot{\hat{\chi}} + p_7 z_3\tan\left(\frac{z_3}{\varepsilon}\right)\right) - \frac{1}{p_4}\tilde{M}_3\dot{\hat{M}}_3 - \frac{1}{p_5}\tilde{l}_{3,2}\dot{\hat{l}}_{3,2} + \xi\dot{\xi} \\
&\le -k_5 z_3^2 - k_6 z_3\,\mathrm{sig}^{\gamma_4}(z_3) - \tau z_3 z_2 + \lambda\delta_1 + z_3 k_7\xi + \kappa\chi\varepsilon + z_3 b\rho\Delta v \\
&\quad + |z_3|\tilde{M}_3 + |z_3|\tilde{l}_{3,2} - \tilde{M}_3\left(|z_3| - l_4\hat{M}_3\right) - \tilde{l}_{3,2}\left(|z_3| - l_5\hat{l}_{3,2}\right) + \frac{\lambda l_6}{p_6}\tilde{\ell}\dot{\tilde{\ell}} + \frac{1}{p_7}\tilde{\chi}\dot{\tilde{\chi}} + \xi\dot{\xi} \\
&\le -k_5 z_3^2 - k_6 z_3\,\mathrm{sig}^{\gamma_4}(z_3) - \tau z_3 z_2 + \lambda\delta_1 + \kappa\chi\varepsilon + z_3 b\rho\Delta v + z_3 k_7\xi \\
&\quad + l_4\hat{M}_3\tilde{M}_3 + l_5\hat{l}_{3,2}\tilde{l}_{3,2} + \frac{\lambda l_6}{p_6}\tilde{\ell}\dot{\tilde{\ell}} + \frac{1}{p_7}\tilde{\chi}\dot{\tilde{\chi}} + \xi\dot{\xi}
\end{aligned}
\tag{69}
$$

Substituting (58) into (69) yields

$$
\begin{aligned}
\dot{V}_3 &\le -k_5 z_3^2 - k_6 z_3\,\mathrm{sig}^{\gamma_4}(z_3) - \tau z_3 z_2 + \lambda\delta_1 + \kappa\chi\varepsilon + z_3 k_7\xi + z_3 b\rho\Delta v \\
&\quad + l_4\hat{M}_3\tilde{M}_3 + l_5\hat{l}_{3,2}\tilde{l}_{3,2} + \frac{\lambda l_6}{p_6}\tilde{\ell}\dot{\tilde{\ell}} + \frac{1}{p_7}\tilde{\chi}\dot{\tilde{\chi}} \\
&\quad + \xi\left(-k_8\xi - \frac{|z_3 b\rho\Delta v| + 0.5b\Delta v^2}{|\xi|^2}\xi - b\Delta v - k_9\,\mathrm{sig}^{\gamma_3}(\xi)\right) \\
&\le -k_5 z_3^2 - k_6 z_3\,\mathrm{sig}^{\gamma_4}(z_3) - k_8\xi^2 - k_9\xi\,\mathrm{sig}^{\gamma_3}(\xi) - \tau z_3 z_2 + \lambda\delta_1 + \kappa\chi\varepsilon + z_3 k_7\xi + z_3 b\rho\Delta v \\
&\quad + l_4\hat{M}_3\tilde{M}_3 + l_5\hat{l}_{3,2}\tilde{l}_{3,2} + \frac{\lambda l_6}{p_6}\tilde{\ell}\dot{\tilde{\ell}} + \frac{1}{p_7}\tilde{\chi}\dot{\tilde{\chi}} - |z_3 b\rho\Delta v| + 0.5b\Delta v^2 - \xi b\Delta v
\end{aligned}
\tag{70}
$$

As

$$\begin{aligned} & z_3 k_7 \xi - \xi b \Delta v \le \frac{1}{2} k_7 \left| z_3 \right|^2 + \xi^2 + \frac{1}{2} b \Delta v^2 \\ & z_3 b \rho \Delta v - \left| z_3 b \rho \Delta v \right| \le 0 \end{aligned} \tag{71}$$

According to(71),then(70) can be derived

$$\begin{aligned} \dot{V}_3 \le & -\left(k_5 - \frac{1}{2} k_7 \right) z_3^2 - k_6 z_3 \operatorname{sig}^{\gamma_4} \left(z_3 \right) - \left(k_8 - 1 \right) \xi^2 - k_9 \xi \operatorname{sig}^{\gamma_3} (\xi) - \tau z_3 z_2 + \lambda \delta_1 + \kappa \chi \varepsilon \\ & + l_4 \hat{M}_3 \tilde{M}_3 + l_5 \hat{l}_{3,2} \tilde{l}_{3,2} + \frac{\lambda l_6}{p_6} \tilde{\ell} \hat{\ell} + \frac{1}{p_7} \tilde{\chi} \hat{\chi} \\ \le & -\left(k_5 - \frac{1}{2} k_7 \right) z_3^2 - k_6 z_3 \operatorname{sig}^{\gamma_4} \left(z_3 \right) - \left(k_8 - 1 \right) \xi^2 - k_9 \xi \operatorname{sig}^{\gamma_3} (\xi) \\ & - \frac{1}{2} l_4 \tilde{M}_3^2 - \frac{1}{2} l_5 \tilde{l}_{3,2}^2 - \frac{\lambda l_6}{p_6} \tilde{\ell}^2 - \frac{1}{2 p_7} \tilde{\chi}^2 - \tau z_3 z_2 + \frac{1}{2 p_7} \hat{\chi}^2 \\ & + \frac{\lambda l_6}{2 p_6} \hat{\ell}^2 + \frac{1}{2} l_4 M_3^2 + \frac{1}{2} l_5 l_{3,2}^2 \hat{\chi} + \lambda \delta_1 + \kappa \chi \varepsilon \end{aligned} \tag{72}$$

Computing the derivative of V and applying(40), (53) and(72), yields

$$\begin{aligned} \dot{V} \le & -k_1 z_1^2 - k_3 z_2^2 - \left(k_5 - \frac{1}{2} k_7 \right) z_3^2 - \left(k_8 - 1 \right) \xi^2 - k_2 z_1 \operatorname{sig}^{\gamma_1} \left(z_1 \right) - k_4 z_2 \operatorname{sig}^{\gamma_2} \left(z_2 \right) \\ & - k_6 z_3 \operatorname{sig}^{\gamma_3} \left(z_3 \right) - k_9 \xi \operatorname{sig}^{\gamma_3} (\xi) - \frac{1}{2} l_1 \tilde{M}_1^2 - \frac{1}{2} l_2 \tilde{M}_2^2 - \frac{1}{2} l_3 \tilde{l}_{2,2}^2 - \frac{1}{2} l_4 \tilde{M}_3^2 - \frac{1}{2} l_5 \tilde{l}_{3,2}^2 \\ & - \frac{\lambda l_6}{p_6} \tilde{\ell}^2 - \frac{1}{2 p_7} \tilde{\chi}^2 + \frac{1}{2} l_1 M_1^2 + \frac{1}{2} l_2 M_2^2 + \frac{1}{2} l_3 l_{2,2}^2 + \frac{1}{2} l_4 M_3^2 + \frac{1}{2} l_5 l_{3,2}^2 + \frac{\lambda l_6}{2 p_6} \hat{\ell}^2 \\ & + \frac{1}{2 p_7} \hat{\chi}^2 + \lambda \delta_1 + \kappa \chi \varepsilon \\ \le & -k_1 z_1^2 - k_3 z_2^2 - \left(k_5 - \frac{1}{2} k_7 \right) z_3^2 - \left(k_8 - 1 \right) \xi^2 - \frac{1}{2} l_1 \tilde{M}_1^2 - \frac{1}{2} l_2 \tilde{M}_2^2 - \frac{1}{2} l_3 \tilde{l}_{2,2}^2 - \frac{1}{2} l_4 \tilde{M}_3^2 - \frac{1}{2} l_5 \tilde{l}_{3,2}^2 \\ & - \frac{\lambda l_6}{2 p_6} \tilde{\ell}^2 - \frac{1}{2 p_7} \tilde{\chi}^2 + \frac{1}{2} l_1 M_1^2 + \frac{1}{2} l_2 M_2^2 + \frac{1}{2} l_3 l_{2,2}^2 + \frac{1}{2} l_4 M_3^2 + \frac{1}{2} l_5 l_{3,2}^2 + \frac{\lambda l_6}{2 p_6} \hat{\ell}^2 + \frac{1}{2 p_7} \hat{\chi}^2 \\ & + \lambda \delta_1 + \kappa \chi \varepsilon \\ \le & -\varphi V + \rho \end{aligned} \tag{73}$$

where

$$\begin{aligned} & \varphi = \min\{2k_1, 2k_2, 2(k_5 - \frac{1}{2} k_7), 2(k_8 - 1), l_1 p_1, l_2 p_2, l_4 p_4, l_3 p_3, l_5 p_5, \lambda, 1\} \\ & \rho = + \frac{1}{2} l_1 M_1^2 + \frac{1}{2} l_2 M_2^2 + \frac{1}{2} l_3 l_{2,2}^2 + \frac{1}{2} l_4 M_3^2 + \frac{1}{2} l_5 l_{3,2}^2 + \frac{\lambda l_6}{2 p_6} \hat{\ell}^2 + \frac{1}{2 p_7} \hat{\chi}^2 + \lambda \delta_1 + \kappa \chi \varepsilon \end{aligned} \tag{74}$$

The $e^{\varphi t}$ multiply both sides of equation (73)

$$\left(V(t) + \varphi V(t) \right) e^{\varphi t} \le \rho e^{\varphi t} \tag{75}$$

Form (75) can be derived:

$$V(t) \le \left(V(0) - \Gamma \right) e^{-\varphi t} + \Gamma \tag{76}$$

where $\Gamma = \rho / \varphi$.

Based on the above (76), the inequalities (77) can be hold as:

$$\boldsymbol{z}_{vi} \le \sqrt{V(0)+\Gamma} = \Delta_i (i=1,2,3) \tag{77}$$

Therefore, we conclude that $\boldsymbol{z}_{vi}$ will converge to the region Δ_i in finite time.

Then the Theorem 1 is proved.

4. Simulations

In order to further validate the effectiveness that chaser can realize missile air-intercepting the maneuvering target under the adaptive anti-saturation dynamic surface fault-tolerant control scheme, numerical simulations are conducted in this section.

The missile's initial value: velocity is 1032m/s, initial position $x_m = 0\,\text{km}$, $y_m = 16\,\text{km}$ angle of attack $\alpha(0) = 10^\circ$ $\alpha(0) = 10^\circ$ and flight path angle $\varphi_m = 0^\circ$. The target's initial value initial position $x_t = 1\,\text{km}$, $y_t = 16\,\text{km}$, flight path angle $\varphi_t = 10^\circ$.The maximum the deflection angle of the missile is 30°.

The nominal aerodynamic parameters of the missile are

$$-\frac{57.3qsc_y^{\alpha}}{mV_M} = 0.387, -\frac{57.3qsc_y^{\delta_z}}{mV_M} = 0.068, \frac{57.3qsm_z^{\alpha}}{J_z} = -17.801$$
$$\frac{qsl^2 m_z^{\bar{w}_z}}{J_z V_M} = -0.2741, \frac{57.3qsl^2 m_z^{\delta_z}}{J_z} = -31.26$$

The steering engine model is defined as

$$\frac{\delta_z(s)}{\delta_{zc}(s)} = \frac{1}{0.01s+1}$$

In order to show the effectiveness and robustness of the guidance strategy designed in this paper, the simulation is compared with the [6]. For the purpose of simplicity, the Neural network controller proposed in [6] is abbreviated as NNC. And the targets are divided into two cases to be simulated: constant maneuver and sine maneuver.

Case 1： $a_t = 5g$ **.**

Case 2： $a_t = 7g\sin(t)$.

(1) Simulation analysis for constant maneuvering.

The parameters of adaptive anti-saturation dynamic surface fault-tolerant guidance law(59) are chosen as. $k_1 = k_3 = k_5 = k_7 = k_9 = 0.1$, $k_{30} = 0.6$, $l_1 = l_2 = 0.02$, $l_3 = l_4 = l_5 = l_6 = l_7 = 0.02$, $\eta = 0.01$ $r_1 = r_2 = r_3 = r_4 = 0.05$, $\gamma_1 = \gamma_2 = \gamma_3 = \gamma_4 = 0.65$, $p_1 = p_2 = p_3 = p_4 = p_5 = p_6 = p_6 = 0.01$, $k_2 = 0.05$, $k_4 = k_6 = k_8 = 0.05$. To show the robustness of the proposed method, the time-varying factor of actuator

faults are assumed as $u = 0.1\sin t * \mathrm{sat}(v) + 0.3$.The simulation curves of the missile-target are shown in Figs.2(a)-(f). Table 1 presents the miss distances for two cases, and also reveals interception times

Table 1 Miss distances and interception times

Guidance laws	The kinds of target accelerations	Miss distance(m)	Interception time(s)
Proposed mehtod	$a_t = 5g$	0.342m	7.652
	$a_t = 7g\sin(t)$	0.76	7.823
NNC	$a_t = 5g$	0.766	7.454
	$a_t = 7g\sin(t)$	0.975	7.812

Fig.2(a)-Fig.2(b) show the relative distance and the trajectories of missile and target under the two control strategies, respectively. And the missile can accurately intercept the targets. From Table 1, we can see that proposes the miss distance of the guidance method when actuator failure occurs in this paper is 0.342 m, which is more precise than the miss distance of 0.76m by the NNC. It can be clearly seen from Fig. 2(c) that for the constant target maneuvers, under the two control schemes, in the initial stage the line-of-sight angle rate can quickly and smoothly converge to the expected neighborhood of expected values. However, under the NNC guidance law the line-of-sight angle rate curve has a large chattering during the convergence process, which will cause a large miss distance (see Table 1). In Fig. 2(d)-Fig. 2(e), the curves of the angle of attack and the pitch angular rate the missile under two guidance strategies are respectively shown. From the results, it can be observed clearly that the angle of attack and pitch angular can meet within the expected value range during the control process under the proposed method, however, the angle of attack under the action of NNC does not meet the state constraint $|z_2| \le 10^\circ$. In Fig. 2(e), the curves of deflection angle under the two guidance laws are given. It can be seen that the deflection angle is bounded in the whole control process without chattering which meet the requirement of input saturation compare with NNC.

Based on the results presented in Fig. 2, it can be concluded that the missile can realize accurately intercepting constant maneuvering target using the adaptive dynamic surface fault-tolerant controller with external disturbances, input saturation, actuator faults, and state constraints.

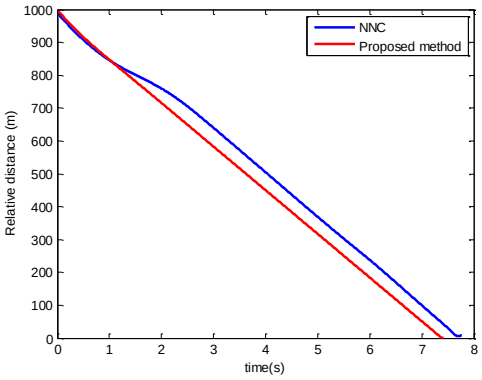

(a) Relative distance

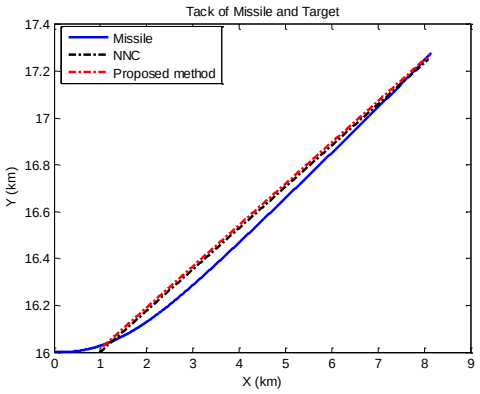

(b) Trajectories of missile and target

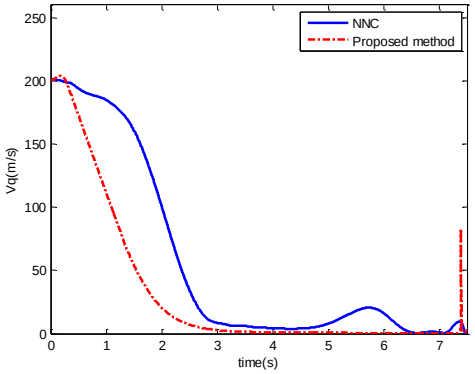

(c)Curve of the line-of-sight angle rate

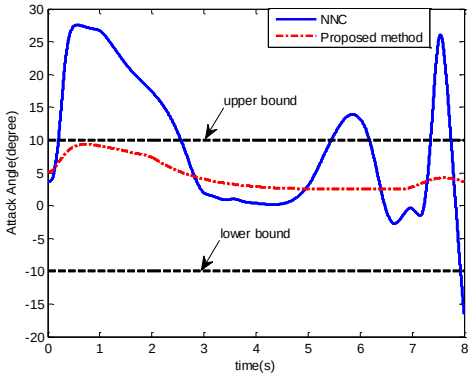

(d) Curve of the angle of attack

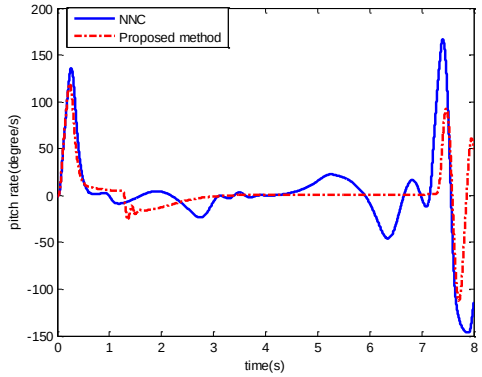

(e) Curve of the angle pitch rate

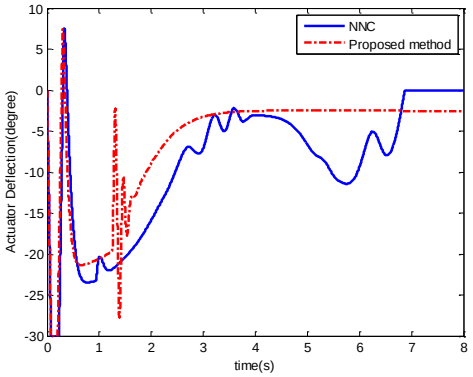

(f) Curve of the deflection angle

Fig. 2 Comparison results under these two guidance laws for case 1

（2）Simulation analysis for snake maneuvering

The control parameters in the simulation analysis of case 2 are the same as in case 1, and the simulation results are shown in Fig. 3.

In Fig.3 (a)-Fig.3 (f), the relative distance, trajectories of missile and target, the curve of line-of-sight rate, the angle of attack and pitch rate and the curve of deflection angle are given. In Fig. 3(a)-Fig. 3(b), it can be seen that under two control strategies, the maneuver target of snake form has a small miss distance and a precise intercept snake target. From Fig. 3(c) it can be seen that the curve of line-of-sight rate converge to a small neighourhood of zero rapidly in finite time, according to the parallel approach method, the effectiveness of the control strategies is demonstrated. In Fig.3(d)-Fig.3(e), it can be seen

that the change range of both the angle of attack and the pitch rate can meet the physical constraint requirements. It can be seen from Fig. 3(f), the compensation term of input constraints is introduced in the proposed method. Compared with NNC, the deflection angle has a smoother and meets the physical requirements of the actuator.

In summary, the guidance strategy designed in this paper is effective for different maneuver target forms.

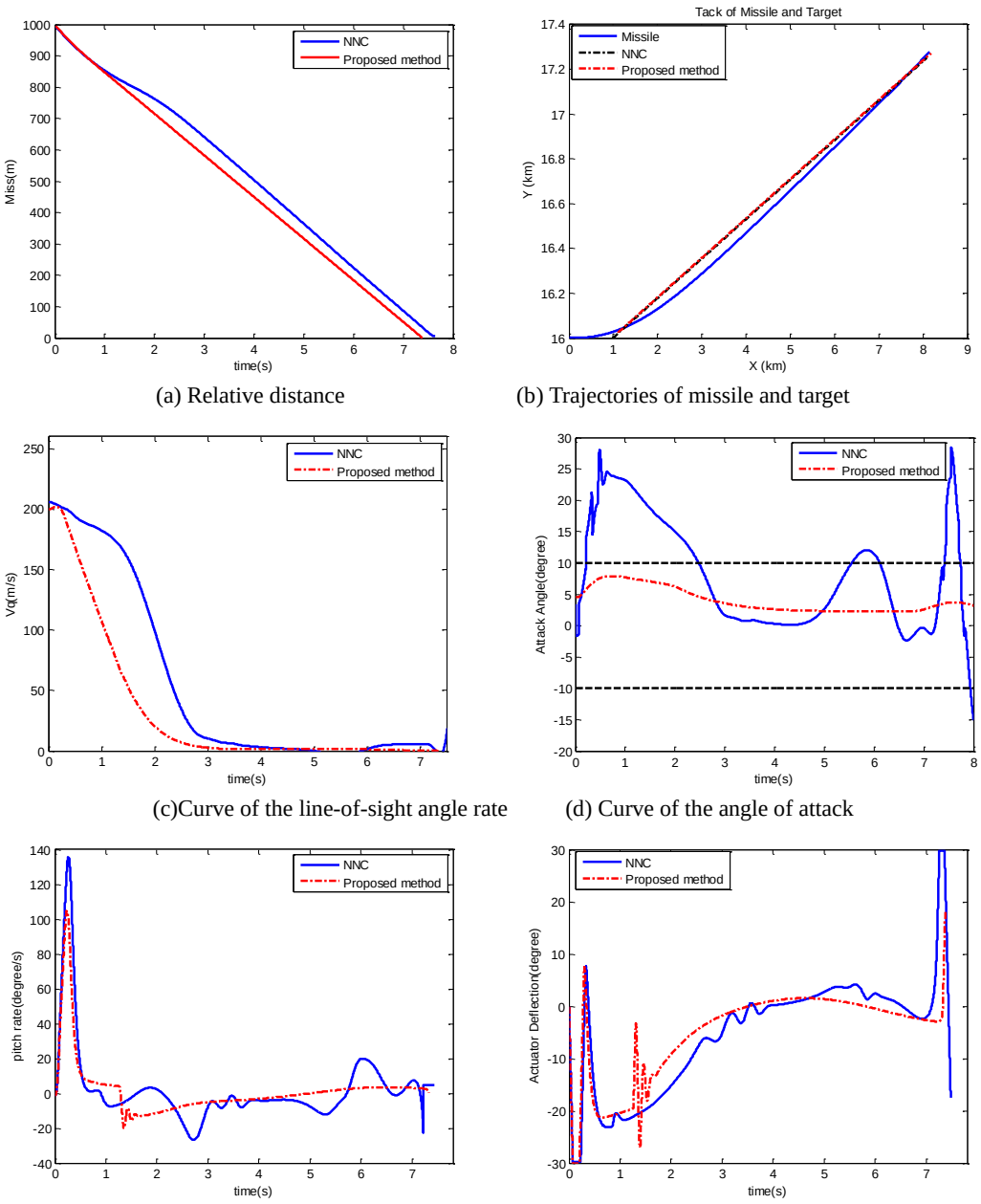

(a) Relative distance (b) Trajectories of missile and target

(c)Curve of the line-of-sight angle rate (d) Curve of the angle of attack

(e) Curve of the angle of pitch (f) Curve of the deflection angle

Fig.3 Comparison results under these two guidance laws for case 2

5. Conclusions

In this thesis, an adaptive dynamic surface fault-tolerant control scheme considering input saturation,

actuator failure, and state constraints is studied and analyzed. The major conclusions of this paper are as follows:

(1) By means of adopting tangent barrier Lyapunov function and auxiliary system in the dynamic surface controller, which can handle partial state constraints and input saturation problem, respectively.

(2) For the situations of unknown upper bound of system disturbances and actuator failures, the adaptive control is adopted to estimate the upper bound of the disturbance and actuator failures which are not required to be known in advance, respectively.

(3) Under the designed fault-tolerant control strategy, according to the theory and simulation results show that when the requirements of input saturation and state constraint are met and targets with different maneuvering forms are intercepted, good guidance precision can be obtained, which indicates the robustness and effectiveness of the designed control scheme.

Acknowledgement

The authors would like to acknowledge the financial support provided by the keypoint research and invention program in Hunan Province of China(2018GK2014).

Conflict of Interests

The authors declare that there is no conflict of interests regarding the publication of this article.

References

[1] Guo, J., Xiong Y, Zhou J. "A new sliding mode control design for integrated missile guidance and control system," Aerospace Science and Technology, Vol.78, 2018, pp. 54-56.

[2] Hou, M, Z. Liang, X, L., Duan, G, Z., "Adaptive block dynamic surface control for integrated missile guidance and autopilot," Chinese Journal of Aeronautics, Vol.26, No.3, 2013, pp.741- 750.

[3] Sun, Y, C., Ma, G, G., "Neural network-based distributed adaptive configuration containment control for satellite formations," Proceedings of the Institution of Mechanical Engineers, Part G: Journal of Aerospace Engineering, Vol.232, No.12, 2018, pp. 2349-2363.

[4] Guo, Y., Guo, J, H., Song, S, M., "Back-stepping control for attitude tracking of the spacecraft under input saturation," Acta Astronautica, Vol.138, 2017, pp.318–325.

[5] Sun, G., Li, D., Ren, X., "Modified neural dynamic surface approach to output feedback of MIMO nonlinear systems," IEEE transactions on neural networks and learning systems, Vol.26, No.2, 2015, pp.224-236.

[6] Zhao, B, Q., Song, S, M., "Integrated playback design of missile guidance and control based on

adaptive sliding-mode control. Journal of Projectiles," Rockets, Missiles and Guidance, Vol.29, No. 5, 2009, pp.31-35.

[7] Dong, C, Y., Cheng, W, Y., Wang, Q., "Back-stepping sliding mode control for integrated guidance and control design based on active disturbance rejection," systems engineer and electronic, Vol.37, No.7, 2015, pp.1604- 1610.

[8] Sun, X, Y., Yao, T., Wang, S, Y., "Integrated Guidance and Control Design Method Considering Channel Coupling," Journal of Astronautics, Vol.8, 2016, pp.937- 945.

[9] Jiang. H., Zhao. G. R., Zhao. Z. X., "Integrated guidance and control design of vehicle based on block diagonal control," Fight Dynamics, Vol.31, No.5, 2013, pp. 437-442.

[10] Sharma. M, Richards. N., "Adaptive, integrated guidance and control for missile interceptors," AIAA guidance, navigation, and control conference and exhibit, 2004, pp.690- 704.

[11] Wang. W., Zhao. B. Q., Dong. J. P., "Integrated back-stepping design of missile guidance and control via adaptive neural network," Aero weaponry, Vol.05, 2012, pp.13-19.

[12] Wang. J. H., Liu. L. H., Zhao. T., "Integrated guidance and control for hypersonic vehicles in dive phase with multiple constraints," Aerospace Science and Technology, Vol.53, 2016, pp.103-115.

[13] Zhu. J., Liu. L., Tang. G., Bao. W., "Three-dimensional nonlinear coupling guidance for hypersonic vehicle in dive phase," Science China Technological Sciences. Vol. 57, No.9, 2014, pp. 1824–1833 .

[14] Xu. J., "Adaptive fault-tolerant control for a class of output constrained nonlinear systems," International Journal of Robust and Nonlinear Control. Vol.25, No.18, 2015, pp.3732–3745.

[15] Xu. J., "Adaptive fault tolerant control for a class of input and state constrained MIMO nonlinear systems," International Journal of Robust and Nonlinear Control. Vol.26, No.2, 2016, pp.286–302.

[16] Sun. J. G., Song. S. S. M., Li. P., "Adaptive anti-saturation fault-tolerant control of hypersonic vehicle with actuator faults," Proceedings of the Institution of Mechanical Engineers, Part G: Journal of Aerospace Engineering, Vol.233, No.6, 2019, pp. 2066-2083.

[17] Wang. C., Wu. Y., Yu. J., "Barrier Lyapunov functions-based dynamic surface control for pure-feedback systems with full state constraints," IET Control Theory & Applications, Vol.11, No.4, 2016, pp.524–530.

[18] Sun. J. G., Xu. S. Li. Song. S. M., Dong. X. J., "Finite time tracking control of hypersonic vehicles with input saturation," Aerospace science and technology, Vol.71, 2017, pp. 272-284.

[19] Sun. J. G., Song. S. M., Wu. G. Q., “Tracking control of hypersonic vehicle considering input constraint”, Journal of Aerospace Engineering, Vol.30, No.6, 2017, pp.1-13.

[20] Guo. Y., Huang, B., Wang, S., “Adaptive Finite-Time Control for Attitude Tracking of Spacecraft under Input Saturation,” Journal of Aerospace Engineering, Vol.31, No.2, 2017.

[21] Dong, W., Farrell, J, A., Polycarpou, M, M., “Command filtered adaptive backstep-ping. Control Systems Technology,” IEEE Transactions on, Vol.20, No.3, 2012, pp.566–580.

[22] Farrell. J., Sharma. M., Polycarpou. M., “Back-stepping-based flight control with adap-tive function approximation,” Journal of Guidance, Control and Dynamics, Vol. 28, No.6, 2005, pp.1089–1102.

[23] Lee. C., Kim. T., Tahk. M., “Polynomial guidance laws considering terminal impact angle and acceleration constraints,” IEEE Transactions on Aerospace and Electronic Systems, Vol.49, No. 1, 2013, pp.74-92.

[24] Wang. W. H., Xiong. S., “Three dimensional impact angle constrained integrated guidance and control for missiles with input saturation and actuator failure,” Aerospace Science and Technology, Vol.53, 2016, pp.169-187.

[25] Fathi. J. M, Ashrafifar. A., Mohsenipour. R., “Adaptive integrated guidance and fault tolerant control using backstepping and sliding mode,” International Journal of Aerospace Engineering, 2015.

[26] Liu, W., Wei, Y., Hou, M., “Integrated guidance and control with partial state constraints and actuator faults,” Journal of the Franklin Institute, Vol.356, No.9, 2019, pp. 4785-4810.